Analysis of fuel retention on MAST by global gas balance

J. Huang[1,2], S. Lisgo[1,3], G. Maddison[1] and the MAST Team[1]

[1.] EURATOM/CCFE Fusion Association, Culham Science Centre, OX14 3DB, Abingdon, UK

[2.] Institute of Plasma Physics, Chinese Academy of Sciences, P.O.Box 1126, 230031, Hefei, Anhui, P.R. China

[3.] ITER Organization, Cadarache, 13108, St Paul-lez-Durance, France

E-mail: juan.huang@ccfe.ac.uk

Abstract. The retention of deuterium fuel during MAST discharges has been studied using the method of global gas balance. The results show that with inter-shot ^{4}He-GDC, the total number of particles retained for a discharge increases with total number of injected particles, and the total retention fraction stays very high, mostly around 80%, and can be almost 100%. However, it is observed that disruptions can reduce the wall inventory. With inter-shot ^{4}He-GDC to recondition surfaces on MAST, the retention for all shots analyzed has not been observed to saturate, while if there is no ^{4}He-GDC before a shot, the following plasma density can become uncontrollable owing to lower wall pumping capacity. This indicates a majority of injected particles is retained in the walls/divertors during each discharge and most of them can be recovered with ^{4}He-GDC, suggesting that on the short time-scale of MAST pulses, the particle balance is dominated by dynamic retention, which is mostly attributed to direct implantation of ions and neutral particles in a shallow surface layer.

Submitted to: *Plasma Phys. Control. Fusion*

PACS numbers: 52.40.Hf, 52.55.Fa

1. Introduction

Evaluation of fuel retention in present tokamaks is one of the most crucial issues for next-step fusion devices, such as ITER, due to safety considerations, which restrict its tritium (T) inventory to a likely figure for the eventual administrative limit of $\sim$ 700g [1]. Presently, most tokamaks use both gas balance and post-mortem methods to investigate fuel retention and its mechanisms, which has produced a good database of retention information for predicting to ITER and reactors [2]. One of the methods, global particle balance analysis, as applied in this paper, can determine the exchange of particles between the walls and plasma, evaluate how many are retained in the walls, and also help to understand plasma density and its control [3]. The common features of hydrogenic retention are observed for long-pulse discharges in most devices with carbon as the main plasma-facing-component (PFC) material [4, 5, 6, 7, 8]. During the pulses, two phases can be distinguished in time: the first phase where the retention rate is decreasing, corresponding to the dynamic retention, which is attributed to direct implantation of ions and neutral particles in a shallow surface region, with possible diffusion/migration into the bulk [4]; and the second phase where it is constant, corresponding to the long-term retention, which is due to deeper implantation and co-deposition [9]. For short plasma discharges, recovery experiments after the shot show that dynamic retention can dominate the particle balance [5].

On the MAST (Mega-Ampere Spherical Tokamak) device, fuel retention experiments have been carried out and analyzed using the method of global gas balance. Due to resistive heating of the central solenoid presently limiting purely inductive current drive to about 500ms, the discharge duration so far is normally less than 700ms. Periodically on MAST, several hours of helium glow discharges with $\sim$ 10% deuterated trimethylborane ($B(CD_3)_3$) are used to deposit an amorphous boron-carbon layer on all contacted areas, which acts as a strong getter for impurities, especially oxygen. During operations, shorter inter-shot helium glow discharge cleaning (^{4}He-GDC) is applied to provide for good and repeatable density control in the next shot. Presently the residual-gas analysis (RGA) system cannot accurately resolve the helium and deuterium at mass 4, so analysis of short-term retention is focused upon in this paper. A unique feature of MAST is its open vessel design, the remote wall creating a large vessel to plasma volume ratio of $\sim$ 8:1, which together with the open and extended divertor geometry promotes substantial neutral-particle populations in the main chamber. Thus, in the gas-balance equation, particles in tank must be included. Using calibration of gas inputs, plus evaluation of neutral-beam sources and the effective speed of torus pumps, gas-balance retention studies can be made for most pulses on MAST.

The gas-balance method used on MAST is described in section 2, including the related measurements and detailed characteristics of MAST. Section 3 shows the results and their interpretation, giving insight into the gross features of the retention on MAST. Temporal evolution during the discharge, including disruption effects, and possible retention mechanisms are discussed. Section 4 gives the summary.

Figure 1. The poloidal cross-section of MAST: different gas fuelling positions labeled from 1 to 8, fast ion gauge (FIG) installed in the outer midplane measuring the pressure in the tank, and five turbo-molecular pumps installed at the outer side below the midplane.

2. Experimental Methods

MAST is a low aspect ratio spherical tokamak (ST) with major radius $R_0 \sim 0.85$ m, minor radius $a \sim 0.65$ m, toroidal magnetic field $B_{\mathrm{T}} \sim 0.5$ T, and so far with a maximum plasma current of 1.4 MA, and up to 3.6 MW of neutral-beam power. A unique feature of MAST is the open vessel design with a total vessel volume $V_{\mathrm{vessel}} \approx 55$ m^3 and its poloidal shaping coils suspended inside the vacuum chamber, as shown in figure 1. Employing an open and extended divertor geometry, it can operate in signal-null (SN) or double-null (DN) configuration. The PFCs materials on MAST are composed of: divertor targets and centre column armour, EK 98 fine-grain graphite; PF coil casings and wall, stainless steel; plus the outer midplane coated with graphite to reduce visible reflections. All surfaces are at about 300 K before each shot.

As noted above, evaluation of the wall particle inventory on MAST must take account of the tank population. The particle-balance equation may hence be written:

$$\int_{t_{\mathrm{prefill}}}^{t} Q_{\mathrm{gas}}(t')\mathrm{d}t' + \int_{t_{\mathrm{prefill}}}^{t} Q_{\mathrm{NBI}}(t')\mathrm{d}t'$$

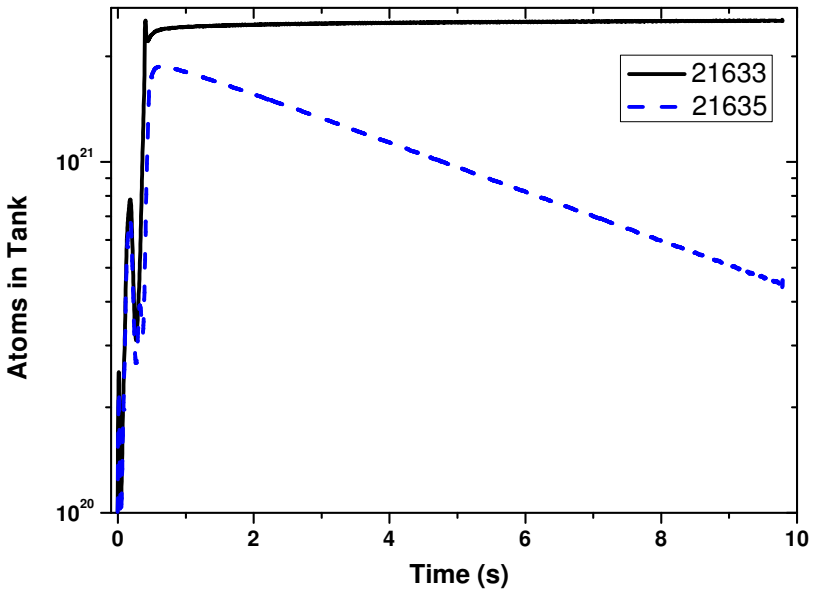

Figure 2. The time evolution of atoms in tank measured by the FIG for: shot 21633 with all pumps closed and shot 21635 with turbo-molecular pumps open.

$$=< n_{\rm e} > (t')V_{\rm plasma}(t') + < n_{\rm tank} > (t')[V_{\rm vessel} - V_{\rm plasma}(t')] + \int_{t_{\rm prefill}}^{t} Q_{\rm wall}(t')\mathrm{d}t' + \int_{t_{\rm prefill}}^{t} Q_{\rm pump}(t')\mathrm{d}t'. \quad (1)$$

where $Q_{\rm gas}$ and $Q_{\rm NBI}$ are the atom injection rates associated with gas puffing and neutral-beam injection, respectively; $< n_{\rm e} >$ is the volume-averaged electron density and $< n_{\rm tank} >$ is the neutral atomic density in the tank; $Q_{\rm pump}$ is the removal rate due to all possible pumping systems of the vessel; and $Q_{\rm wall}$ is the wall pumping rate or release rate. They are calculated from the start of the gas prefilling at time $t_{\rm prefill}$. Thus, the retention fraction $f_{\rm ret}$ can be defined as:

$$f_{\rm ret} = \frac{\int_{t_{\rm prefill}}^{t} Q_{\rm wall}(t')\mathrm{d}t'}{\int_{t_{\rm prefill}}^{t} Q_{\rm gas}(t')\mathrm{d}t' + \int_{t_{\rm prefill}}^{t} Q_{\rm NBI}(t')\mathrm{d}t'}. \quad (2)$$

On MAST, the volume-averaged density can be obtained from Thomson scattering (TS) measurements, either from the multi-time-point Nd:Yag system or from the high-spatial resolution ruby system [10], which are routine measurements, but not continuous ones. Thus the line-averaged plasma density is used instead, which is derived from the vibration-corrected CO_2 interferometer central signal divided by the EFIT path-length. For retention fraction calculation this leads to a systematic error of less than 2%. Confined plasma volume $V_{\rm plasma}$ is interpolated from EFIT reconstruction of the magnetic geometry at 5 ms intervals, but is not available around a disruption.

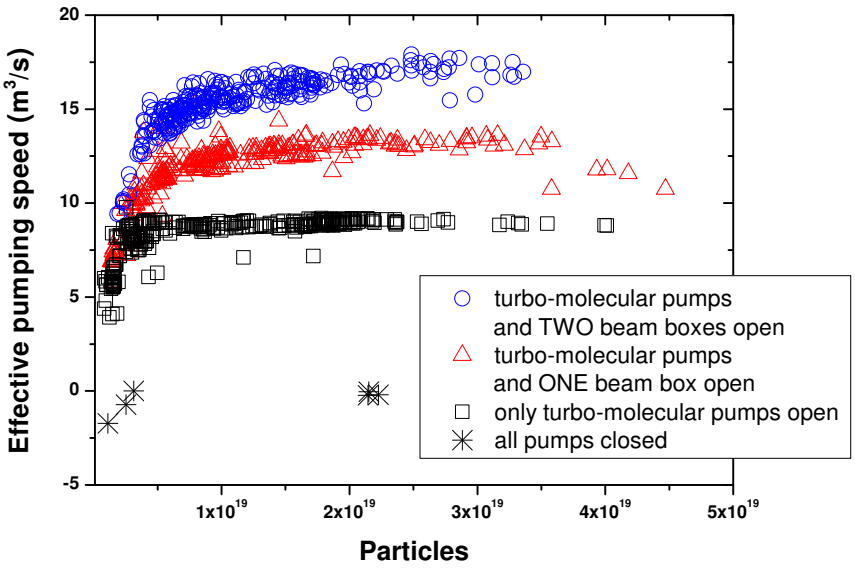

Figure 3. The effective pumping speed as a function of the total number of particles in the tank at $t_0 = 1.5$ s for shots with: turbo-molecular pumps and two beam boxes open (circle symbol), turbo-molecular pumps and one beam boxes open (triangle symbol), only turbo-molecular pumps open (square symbol), and all pumps closed (star symbol) .

There are several optional fuelling positions for gas puffing on MAST, as shown in figure 1. Gas input is specified directly from the voltage waveforms applied to piezovalve inlets, calibrated from ion-gauge measurements of slow pressure evolution when puffing into the tank with no plasma present. To measure particles in the tank during a discharge, a screened Bayard-Alpert fast ionization gauge (FIG) is used, which is calibrated against the same gauge used for piezovalve calibration, as shown in figure 1, installed in the outer mid-plane. Its measurement range is from 10^{-12} to 10^{-6} bar and the duration is limited to 10 s. Comparing FIG measurements against the piezovalve drive waveforms shows that the gas densities taken from the FIG involve an intrinsic time-delay of about 30-35 ms before they respond fully to the programmed waveforms, due to its own time response combined with the shorter time for pressure in the tank to become uniform. Thus the particle balance cannot be determined accurately on time-scales of this order around any large changes in the piezovalve drive waveforms. For the sources from the neutral-beam injection, there are two JET-style Positive Ion Neutral Injectors (PINIs) on MAST and both injectors together presently provide around 3.6 MW of neutral-beam power [11]. Each beam injection rate is calculated to be around 10^{20} atoms/s, while the average gas injection rate is one or two orders higher and is consequently the dominant contribution.

For pumping systems on MAST, there are five turbo-molecular pumps (each with

nominal pumping speed: 2.2 m^3/s) installed on the vessel at the outboard lower side with an aperture of 400 mm and pipe length 200 mm. For the molecular gas flow, the high conductance leads to the effective pumping speed for all turbo-molecular pumps of $\approx$ 10.7 m^3/s. Other possible main sinks are titanium sublimation pumps (TSPs), also known as beam-box getter pumps. Each beam has two getter pumps (each with nominal pumping speed: 150 m^3/s), which are in separate tanks: one pipe connecting the tank for tokamak plasma and that for one of two getter pumps is with an aperture around 300 mm and length 1290 mm, and the other pipe between two tanks for each getter pumps is with the aperture 320 mm and length 210 mm. The total effective pumping speed of the beam-box getter pumps for each PINI is calculated as $\approx$ 6.8 m^3/s. During plasma operations, other pumps may be active too, such as those for diagnostics (reciprocating probe, Thomson scattering, neutral-particle analyzer, etc), which makes the calculation of the effective pumping speed more difficult. Experimentally, an easier way is to measure the effective pumping speed on MAST according to the exponential decay of the particles in the tank after a discharge, shown in figure 2 for the ohmic shot 21635 with only turbo-molecular pumps on and shot 21633 with all pumps closed. According to $P = P_0 e^{-(t-t_0)/\tau_{\rm pump}}$, ($P_0$: the pressure at time t_0 when the exponential decay fit is started, $\tau_{\rm pump}$: the decay time due to the pump), the effective pumping speed $S_{\rm e} = V_{\rm vessel}/\tau_{\rm pump}$, is evaluated as $\sim$ 9 m^3/s. By the same method, the effective pumping speeds for shots 20673 to 22567 were evaluated as a function of the total number of atoms in the tank at $t_0 = 1.5$ s after the termination of the discharge. Figure 3 shows three branches ($\sim$ 9 m^3/s, $\sim$ 13 m^3/s, $\sim$ 17 m^3/s) for most of the discharges and those values around zero correspond to shots with all pumps closed. The square, triangle and circle symbols correspond to the shots with only turbo-molecular pumps open, with turbo-molecular pumps and one beam box open, and with turbo-molecular pumps and two beam boxes open, respectively. It shows that for turbo-molecular pumps, the effective pumping speed is measured as $\sim$ 9 m^3/s, and for each of the two PINIs, the effective pumping speed of beam-box getter pumps is $\sim$ 4 m^3/s. The measurements are consistent with the above theoretical values. This graph indicates that presently on MAST, the main active pumps are the turbo-molecular and beam-box getter pumps, and for the particle balance calculation, these measured effective pumping speeds are used in this paper. During the shot, the neutral beam could block the box to tank aperture, and getter pumping speed of the tank can be even lower. However, from the analysis below, it is found that the number of total pumped particles during a discharge is very small compared to that of the total injected particles.

3. Experimental results and discussion

Retention has been calculated for MAST plasma shots from 20673 to 22567, except those with helium or impurity gas puffing. Here, it should be noted that MAST generally adopts a 'soft-stop' to each plasma discharge. That is, when the solenoid current is saturated, an amount of gas puff will be triggered until the plasma current ends, aiming

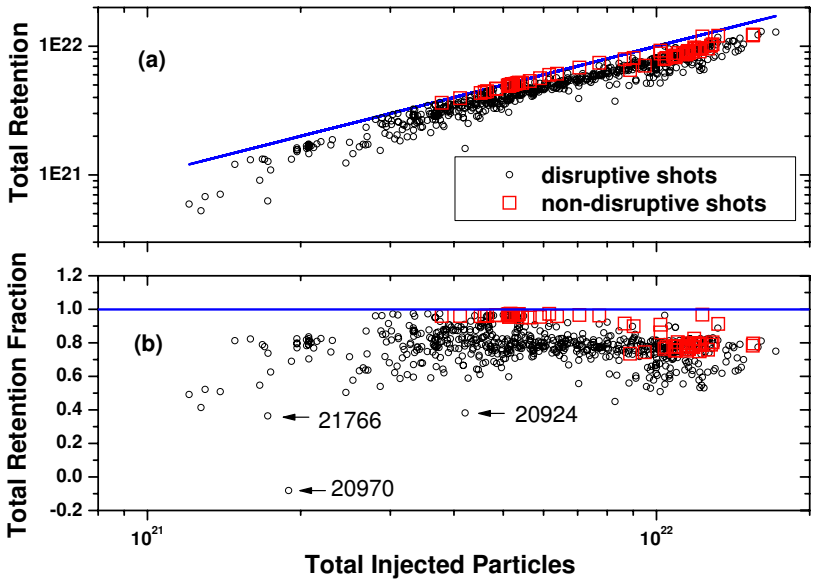

Figure 4. (a) The total retention of the discharge, and (b) the total retention fraction of the discharge as a function of the total number of injected particles (circles: disruptive shots, squares: non-disruptive shots, shot 20970, 20924 with disruption before the solenoid current saturated and shot 21766 without preceding ^{4}He-GDC are discussed in the text).

to make the plasma terminate smoothly. When the solenoid runs out of flux, the main priority is to return the solenoid current to zero as quickly as possible to avoid overheating. This induces a strong negative loop voltage, which tends to drive reverse current in the edge of the plasma. This tends to be unstable and to cause a disruption. If a large amount of gas is injected then it tends to cool the plasma and so the current diffuses more rapidly and thus becomes more uniform. So, in most cases injecting a large amount of gas helps to reduce the plasma current to zero quickly without disruption. However, it does not always work and it is possible to exceed the density limit which will also cause a disruption.

3.1. Total retention of the discharges

Figure 4 shows the total number of retained particles and the total retention fraction after each discharge as functions of the total number of injected particles, and figure 5 shows the evolution of the retention fraction as a function of discharge duration. Squares correspond to non-disruptive shots, circles to disruptive ones with the disruption occurring when the current was still above 150-200kA, showing that most of the shots are disruptive. It shows that the total number of retained particles increases with the total amount of injected ones (figure 4(a)), and the retention fractions for most shots are very high (figure 4(b)). Most of them are around 80% and some approach near to 100%. It is

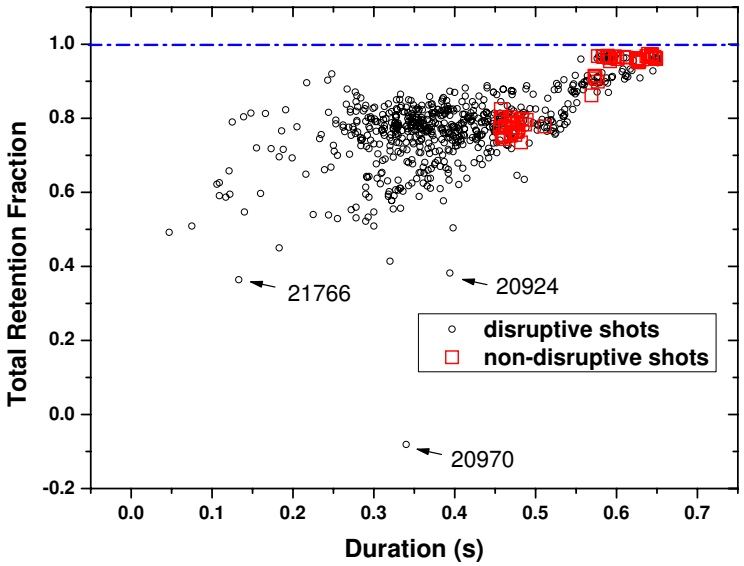

Figure 5. The total retention fraction of the discharge against the discharge duration (circles: disruptive shots, squares: non-disruptive shots, shot 20970, 20924 with disruption before the solenoid current saturated and shot 21766 without preceding ^{4}He-GDC are discussed in the text).

clearly seen that most of the injected particles go into the walls/divertors. In previous work [12], using global modelling to calculate the wall adsorption, it was also shown the particle balance is completely dominated by the wall inventory. With inter-shot ^{4}He-GDC, it is apparent that saturation of wall sinks has not yet been observed.

From analysis of time evolution of the retention below, it is found that during the flat-top of the plasma current, the retention fraction is always kept $\geq$ 90%. For those non-disruptive shots with the total retention fraction around 80% (figure 5), it emerges that this drop in retention fraction at shorter durations is because of their more commonly triggered large gas injection after the solenoid runs out of flux. For the disruptive shots, in addition to these similar behaviours, more scattered points with lower f_{ret} ($< 70\%$) are observed, suggesting that the disruption could potentially reduce the retention.

3.2. Time evolution of the retention during the discharge

3.2.1. Non-disruptive discharges Figure 6(a)(b) shows the time traces of two non-disruptive Ohmic shots with different durations (21859: $\sim$ 600 ms, 20964: $\sim$ 500 ms): plasma current (I_{P}) and line-averaged plasma density (n_{e}), solenoid current (I_{S}) and gas injection rate (Q_{gas}) (with wall retention rate (Q_{wall}) for shot 20964), each component in the particle balance (*plasma*: electrons in plasma, *source*: the number of injected

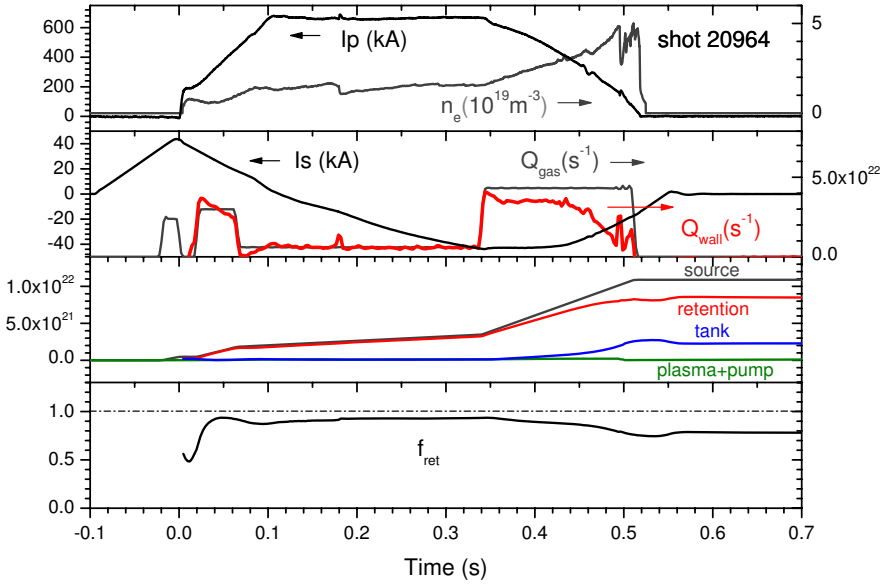

(a)

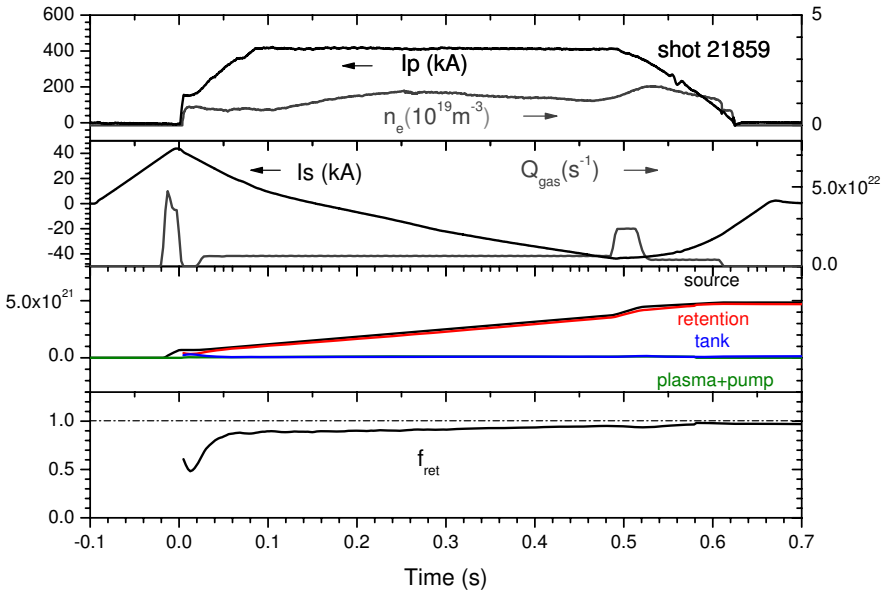

(b)

Figure 6. Time traces for non-disruptive shot 20964 (a) and 21859 (b): plasma current (I_{P}) and line-averaged plasma density (n_{e}), solenoid current (I_{S}) and gas injection rate (Q_{gas}) (with wall retention rate (Q_{wall}) for shot 20964), each component in the particle balance (*plasma*: electrons in plasma, *source*: the number of injected atoms, *tank*: the number of atoms in the tank, *pump*: the number of atoms pumped out, and *retention*: the number of atoms retained in the wall), and the retention fraction f_{ret}.

atoms, *tank*: the number of atoms in the tank, *pump*: the number of atoms pumped out, and *retention*: the number of atoms retained in the walls/divertors), and the retention fraction f_{ret}. During the flat-top, it is seen that the retained inventory is the dominant component in the particle balance, and the retention fraction remains very high ($\geq 90\%$). After the discharge, the retention fraction of shot 20964 drops to $\sim 80\%$, while for shot 21859 it reaches near to 100%. This drop is due to the 'soft-stop' operation. When the solenoid runs out of flux, gas puffing is triggered: for shot 20964, the total triggered gas amount ($\sim 6\times10^{21}$ atoms) is much larger than that of shot 21859 ($\sim 8\times10^{20}$ atoms). During the current ramp down for shot 20964 with the higher injection rate ($\sim 4.5 \times 10^{22}$ atoms/s), considering times after the intrinsic delay of 30-35 ms for the FIG, the wall retention rate Q_{wall} shown in figure 6(a) is $\sim 3.5 \times 10^{22}$ atoms/s and then decreases with time, while during the steady state of the discharge, it reaches nearly the same level as the injection rate. For those analyzed non-disruptive shots, the more common triggering of injection of a large amount of gas for shorter discharges after the solenoid runs out of flux explains why the shorter non-disruptive shots (figure 5) exhibit a retention fraction which drops to around 80%, while at the same time the wall inventory still goes on rising.

3.2.2. Disruptive discharges Figure 7(a)(b) shows two disruptive shots: one where the disruption occurred before the solenoid current saturated (shot 20924), and the other where it occurred afterwards (shot 22236). It is clearly seen that for 20924 there is no gas puff around the disruption, while for 22236 a large input of particles is triggered. During the flat-top period, in both cases the retention fraction remains very high ($\sim 90\%$). For shot 22236, a large amount of triggered gas made the plasma density exceed the density limit which caused a disruption, the retention level after the disruption staying the same as that before the disruption. In contrast, for shot 20924 around the end of the plasma current with no gas puff triggered, the retention drops by 50% after the disruption and the retention fraction decreases from $\sim 90\%$ to $\sim 40\%$ (shown in figure 4 and figure 5), indicating there was net out-gassing due to the disruption, ie overall it can remove particles adsorbed into the walls. Disruptions heat surfaces leading to enormous enhancements of deuterium diffusivity and detrapping rates, thus freeing fuel particles from traps and transporting them to the surface, where they are released [13].

3.3. Discussion

From all discharges above, wall saturation is not observed with inter-shot ^{4}He-GDC conditioning. The high fraction of retained particles can be recovered by inter-shot ^{4}He-GDC, which then provides good and repeatable density in the next shot. On the other hand, if there is no ^{4}He-GDC before a shot, it can lead to uncontrollable plasma density due to lower wall pumping capacity. Figure 8 compares the traces of two shots, 20818 with 8 min of preceding GDC and 21766 with no GDC before. Despite the lower gas puff of shot 21766, its density rose very quickly and exceeded that of shot 20818. Similarly,

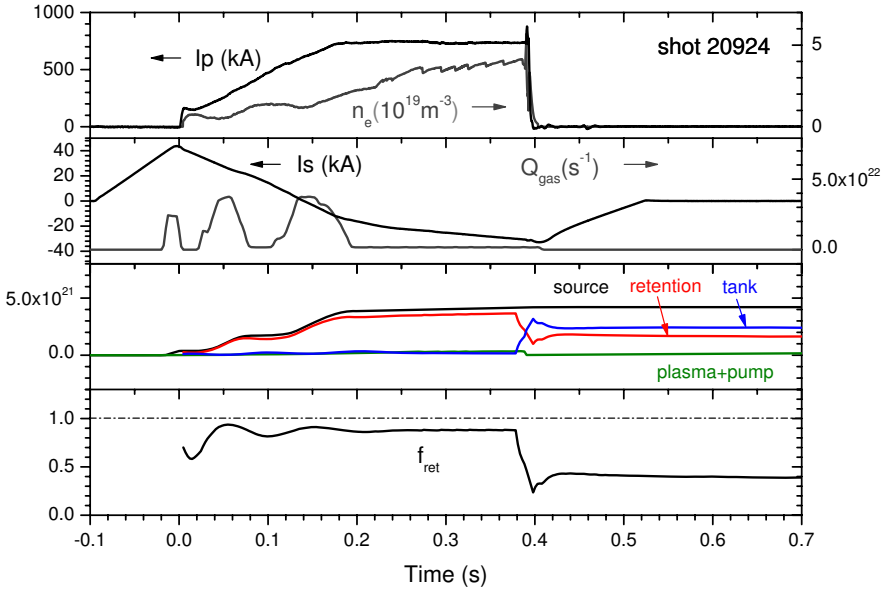

(a)

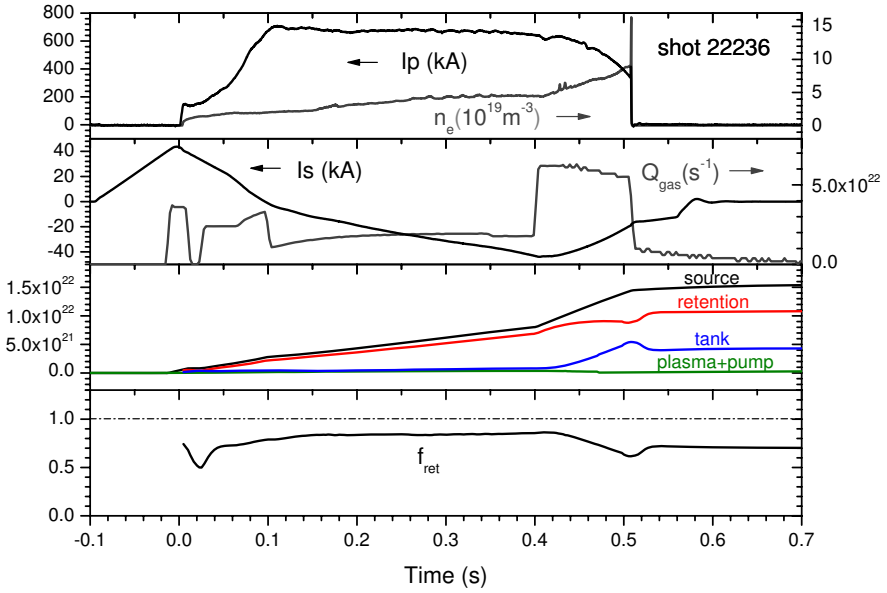

(b)

Figure 7. Time traces of disruptive shots 20924 (a) and 22236 (b) (with the description same as figure 6).

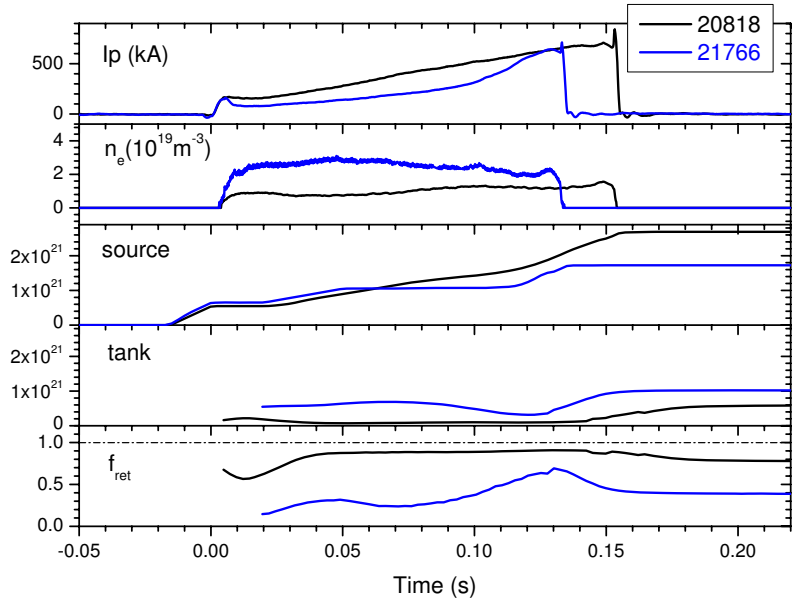

Figure 8. Time traces of two shots: 20818 with 8 min of preceding ^{4}He-GDC and 21766 with no ^{4}He-GDC before: plasma current (I_P), line-averaged plasma density (n_e), *source*: the number of injected atoms, *tank*: the number of atoms in tank, f_{ret}: the retention fraction .

it had higher particle inventory in the tank (figure 8). The retention fraction f_{ret} for shot 21766 is much lower, less than 50% (shown in figure 4 and figure 5), while for shot 20818 it is around 90 %, which indicates the wall pumping capacity for shot 20818 with GDC is much stronger than that for shot 21766 without GDC. From figure 8, for MAST these retained particles from the previous shot lower the wall pumping effect, taking it out of direct density control. Thus, on MAST, out-gassing between discharges without ^{4}He-GDC plays a weak role in the particle balance. However, for most of its shots with preceding ^{4}He-GDC conditioning, the wall-retained particles can be recovered, suggesting mainly dynamic retention. Because ^{4}He-GDC can only remove the short-term retained particles from areas which it can access and where the implantation is shallow [4], its impact is consistent with dominance of dynamic retention on MAST. For short pulses on other devices, the residual inventory accumulated over the day can be compensated by overnight ^{4}He-GDC, yielding an overall balance close to zero [5]. For the analyzed MAST discharges, even nearly complete wall depletion can exist, eg. shot 20970 shown in figure 4(b) and figure 5, also indicating the major portion of the particles is retained temporarily. Evidence of close to saturation with no preceding ^{4}He-GDC and high fraction of retained particles easily recovered by ^{4}He-GDC, suggests long-term retention is small. However, the fraction of long-term retained particles is not known, and the high-mass-resolution analysis of gases in the vacuum tank will next be used to study it further.

4. Summary

Fuel retention has been studied on MAST using the method of global gas balance. The results show that the total number of retained particles increases with total injected ones with inter-shot ^{4}He-GDC and the retention is dominant in the global particle balance. During each discharge, the retention fraction $f_{\rm ret}$ stays very high ($\geq 90\%$). While most of the total retention fractions at the end of each shot are around 80% some of them are much lower, due to: 1) the 'soft-stop' operation, which triggers a large amount of gas after the solenoid runs out of flux; 2) disruption, which can reduce the wall inventory; 3) lower wall pumping capacity, for those shots without ^{4}He-GDC. On MAST the large fraction of retained particles can be recovered by inter-shot ^{4}He-GDC, which provides for good and repeatable density in the next shot. However, if there is no prior ^{4}He-GDC, the following shot can inherit the large amount of particles retained during the previous one, lowering the wall pumping capacity. This suggests retention on MAST is dominated by dynamic effects, allowing most particles to be recovered by ^{4}He-GDC.

Acknowledgments

This work was funded by the UK EPSRC under grant EP/G003955 and the EC under the contract of Association between EURATOM and CCFE. The views and opinions expressed herein do not necessarily reflect those of the European Commission.

References

[1] Roth J. *et al* 2008 *Plasma Phys. Contro. Fusion* **50** 103001 (20pp)
[2] Loarer T. *et al* 2009 *J. Nucl. Mater.* **390-391** 20–28
[3] Bucalossi J. *et al* 2001 *Proc. 28th EPS Conf. on Contr. Fusion and Plasma Phys.* Funchal
[4] Loarer T. *et al* 2007 *Nucl. Fusion* **47** 1112–1120
[5] Tsitrone E. 2007 *J. Nucl. Mater.* **363-365** 12–23
[6] Mertens V. *et al* 2003 *Proc. 30th EPS Conf. on Contr. Fusion and Plasma Phys.* St Petersburg
[7] Loarer T. *et al* 2003 *Proc. 30th EPS Conf. on Contr. Fusion and Plasma Phys.* St Petersburg
[8] Asakura N. 2004 *Plasma Phys. Contro. Fusion* **46** B335–47
[9] Federici G. *et al* 2001 *Nucl. Fusion* **41** 1967–2137
[10] Walsh M.J. *et al* 2003 *Rev. Sci. Instru.* **74** 1663–6
[11] Homfray D.A. *et al* 2009 *Proceedings of the 23rd Symosium of Fusion Engineering* San Diego, California
[12] Maddison G.P. *et al* 2006 *Plasma Phys. Contro. Fusion* **48** 71–107
[13] Lipschultz B. *et al* 2009 *Nucl. Fusion* **49** 045009 (18pp)
[14] Delchambre E. 2007 *J. Nucl. Mater.* **363-365** 1409–13